THE JOURNAL OF PHYSICAL CHEMISTRY LETTERS
A JOURNAL OF THE AMERICAN CHEMICAL SOCIETY

pubs.acs.org/JPCL

Letter

Melt-Processed Halide Perovskite Thin Films from a Two-Dimensional Ruddlesden–Popper Phase Precursor

Atefe Hadi, Rainie L. Schlichtmann, Matthew I. Milot, Jonathan Slobidsky, Madeleine Wilsey, Alex Verburg, Yunhua Chen, Umar H. Hamdeh, Bradley J. Ryan, Brett Boote, Javier Vela, and Matthew G. Panthani*

Cite This: *J. Phys. Chem. Lett.* 2023, 14, 5194–5202

Read Online

ACCESS | Metrics & More | Article Recommendations | Supporting Information

ABSTRACT: While halide perovskite thin films have enormous potential for photovoltaics and other optoelectronics, the use of environmentally hazardous solvents during their deposition and processing poses a barrier to their commercialization. In this work, we demonstrated the deposition of melt-processable precursors and subsequent transformation into halide perovskite thin films without using environmentally hazardous solvents. We melted the wide-bandgap layered perovskites $[(C_6H_5CH(CH_3)CH_2NH_3)_2PbI_4$:$\beta$-Me-$PEA_2PbI_4]$ at ~210 °C and blade coated them into films. The β-Me-PEA_2PbI_4 films were subsequently transformed to perovskite-phase methylammonium or formamidinium lead iodide films using a cation-exchange process in an alcohol-based solvent. Lastly, we demonstrate the potential and limitations of a completely solvent-free approach that uses solid-state transformation of a β-Me-PEA_2PbI_4 film. This work represents a substantial step toward eliminating environmentally hazardous solvents and enables inexpensive industrial-scale liquid-phase deposition processes that do not require expensive systems for handling and disposing of environmentally hazardous solvents.

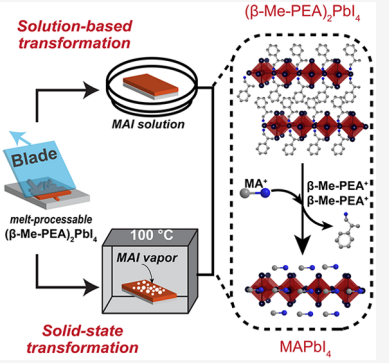

Recent advances in solution-processable lead halide perovskites have demonstrated their promise for photovoltaic (PV) and other optoelectronic applications.[1−8] Solution-based deposition methods offer the potential for dramatically lower capital costs for industrial-scale deposition of the PV absorber layer. However, the low cost associated with laboratory-scale solution deposition does not necessarily apply to industrial solvents as a result of large expenses related to recovering and disposing of toxic solvent vapors. While the toxicities of different solvents vary, typical solvents that are used for depositing halide perovskite thin films, such as dimethylformamide (DMF) or its substitutes,[9] have been classified by many regulatory agencies to be hazardous to the environment. The United States Environmental Protection Agency, for example, classifies these solvents as "air-toxic" solvents or (equivalently) as "hazardous air pollutants".[10] The added capital costs for solvent recovery and disposal are a factor that prevents solution-processable wide-area halide perovskite films and devices from being realized, pointing toward a need for deposition methods that do not require air-toxic solvents.

It is known that some hybrid organic/inorganic Ruddlesden–Popper (RP) phases can melt into the liquid phase without decomposition. Most reported hybrid organic/inorganic RP phases are layered materials that contain a halide perovskite sublattice and have a general formula of $(RNH_3)_2A_{n-1}B_nX_{3n+1}$, where RNH_3 is an aliphatic or aromatic "spacer" cation [e.g., *n*-butylammonium (BA^+) or phenethylammonium (PEA^+)], A is a smaller cation [e.g., methylammonium (MA^+), Cs^+, or formamidinium (FA^+):HC$(NH_2)_2^+$], B is a divalent metal (e.g., Ge, Sn, or Pb), and X is a halide (Cl, Br, or I). The index *n* defines the thickness of metal halide slabs that are confined between RNH_3^+ spacer cations.[11−15] There are a few known hybrid organic/inorganic haloplumbates that undergo melting,[16−19] but many also begin to decompose when heated to temperatures required to melt them. In the early 2000s, Mitzi and co-workers demonstrated that RP phase $(PEA)_2SnI_4$ could be melted and compressed between two substrates to form a solid film upon cooling.[16] Recently, a similar approach was applied to synthesize homologous Pb-based compounds that also melt at temperatures ranging from 207 to 261.4 °C.[17−19] The ability to melt process these compounds arises from a relatively low melting point and sufficiently large gap between their melting and decomposition temperatures.[16−19] In contrast to three-dimensional (3D) halide perovskites, RP phases with $n = 1$ [i.e., $(RNH_3)_2BX_4$] are known to accommodate a wide variety of

Received: December 27, 2022
Accepted: April 27, 2023
Published: May 31, 2023

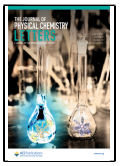

https://doi.org/10.1021/acs.jpclett.2c03916
J. Phys. Chem. Lett. 2023, 14, 5194−5202

spacer cations, and this compositional flexibility can be used to tailor the thermal properties, including their melting temperatures.[16,19,20] For example, $(RNH_3)_2PbI_4$ compounds with short alkylammonium chains (i.e., butylammonium) partially decompose when heated above ∼220 °C, while compounds prepared using many PEA^+-based spacer cations or their derivatives melt without decomposing.[17,19] Other research groups have also identified other solvent-free processing, such as the use of reactive polyiodide melts.[1,2]

While these meltable RP-based compositions could be interesting for solvent-free, liquid-based processing of thin films, their potential for use in PV and other optoelectronic applications is limited as a result of their relatively wide band gaps (>2 eV).[21] Additionally, they tend to crystallize into films that have preferred orientation with corner-sharing octahedral sheets that lie parallel to the substrate; this type of structure is known to hinder charge transport in the vertical (out-of-plane) direction.[13,22,23] A-site cation exchange has been a common procedure in tuning the optical properties of perovskite thin films and nanocrystals.[24−31] Prior reports have demonstrated that immersing $(IC_2H_4NH_3)_2PbI_4$ thin films into a solution of methylammonium iodide (MAI) dissolved in the mixture of isopropanol (IPA) and toluene resulted in the formation of $(IC_2H_4NH_3)_2(CH_3NH_3)_{n-1}Pb_nI_{3n+1}$ with greater degrees of stacking order and higher dimensionality compared to the parent material.[32] This cation exchange was not limited to MAI solution with $IC_2H_4NH_3^+$ spacer cations. PEA_2PbI_4 thin films also transformed to $FAPbI_3$ upon exposure to formamidinium iodide (FAI) solution in IPA.[33] While these approaches are simple and feasible to form a perovskite phase, they still use air-toxic solvents, such as DMF, during the deposition of the precursor phase into thin films, thus posing economic and environmental challenges on an industrial scale.

Here, we aimed to demonstrate the potential of melt-processable precursors by combining melt processing with an A-site cation-exchange approach to tune their structure and optical properties. We focused on β-Me-PEA_2PbI_4 [β-Me-PEA^+ = $C_6H_5CH(CH_3)CH_2NH_3$], which is known to form a stable liquid phase at relatively low temperatures (207 °C).[19] We blade coated melted β-Me-PEA_2PbI_4 onto a substrate to create a film and compared the structure and optical properties of blade-coated films to films prepared by both press coating[19] and spin coating with a conventional, air-toxic solvent. We explored different approaches to cation exchange to replace the β-Me-PEA^+ cations with smaller (FA^+ or MA^+) cations on films prepared using blade and spin coating. We characterized changes in the properties and structure of films using ultraviolet−visible−near-infrared (UV−vis−NIR) absorption spectroscopy (reported as optical absorptance for clarity), photoluminescence (PL), X-ray diffraction (XRD), and scanning electron microscopy (SEM). We gained insight into the kinetics of the cation-exchange process and noticed that a complete conversion of β-Me-PEA_2PbI_4 to $MAPbI_3$ occurred in a few minutes for thinner spin coating. In contrast, the thicker blade-coated films had slower transformation to the 3D perovskite phase of $MAPbI_3$. In addition, we found that prolonged exposure of spin-coated films into FAI solution resulted in the formation of the non-perovskite δ-$FAPbI_3$ phase. In addition to a liquid-based cation exchange, we report a solid-state approach to transform melt-processable precursors into $MAPbI_3$, demonstrating a proof-of-concept technique that could potentially remove the need for any solvents during film deposition and processing. Our work demonstrates that, in concept, semiconducting halide perovskite films with tunable properties may be formed using a melt-based approach that does not use toxic solvents. If the film thickness and morphology of blade-coated films could be optimized, this solvent-free process may be a promising route for depositing halide perovskite films for applications, such as solar cells. Our findings may be more readily applied to the many applications where hybrid perovskite films do not require smooth, conformal films with precisely defined thickness, such as colorimetric sensors,[34] scintillators,[35,36] chemical sensing,[37] and memory devices.[7,38]

Scheme 1a illustrates the process that we used for depositing β-Me-PEA_2PbI_4 films (see Figure S1 of the Supporting Information, a photograph of the experimental apparatus). We used blade coating as a result of its similarity to techniques used for depositing films on wide-area substrates that would be utilized in industrial PV manufacturing. Furthermore, unlike previously used press-coating techniques, blade-coating leaves the top surface of the film uncovered, allowing for further processing and fabrication of nonplanar devices, such as solar cells. To deposit β-Me-PEA_2PbI_4 films, we placed β-Me-PEA_2PbI_4 powder on TiO_2-coated fluorine-doped tin oxide (FTO) substrates and placed the substrate on a heating stage set to 210 °C, allowing the powder to melt. The liquid was then immediately blade-coated, and the substrate was quickly removed from the heating stage to avoid prolonged heating of the β-Me-PEA_2PbI_4 film, which we found to result in partial decomposition to PbI_2 (Figure S2 of the Supporting Information).

Scheme 1. Illustration of the Process Used To Melt Process β-Me-PEA_2PbI_4 and Subsequently Transform the Melt-Processable Precursor to 3D Perovskite Films: (a) Blade Coating of Melted β-Me-PEA_2PbI_4 Followed by (b) Cation Exchange, Where a Solution-Based Exchange of Methylammonium Iodide (CH_3NH_3I, MAI) Dissolved Solution Is Shown, Resulting in a (c) Transformation to a $MAPbI_3$ Film

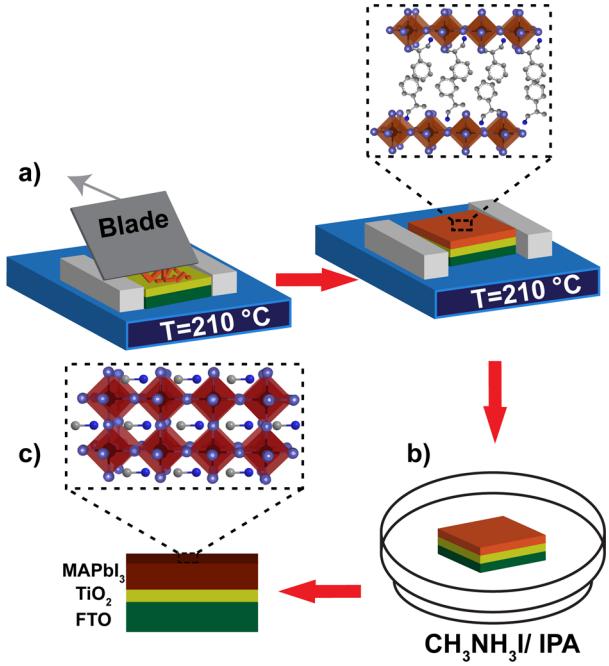

https://doi.org/10.1021/acs.jpclett.2c03916
J. Phys. Chem. Lett. 2023, 14, 5194−5202

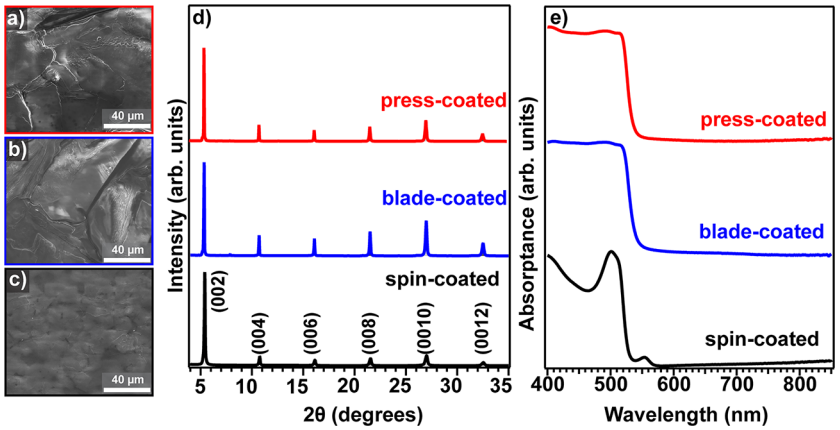

Figure 1. SEM images of (a) press-coated, (b) blade-coated, and (c) spin-coated β-Me-PEA_2PbI_4 films and XRD and absorptance spectra are shown in panels d and e, respectively.

The morphology of the blade-coated films depended upon the processing conditions, including the substrate and blade temperature, blade properties, and translation speed of the stage. Initial attempts of using various room-temperature blade materials, including stainless-steel razor blades, glass, and Teflon, resulted in films with high degrees of visible surface roughness (Figure S3 of the Supporting Information) and were microscopically inhomogeneous (Figure S4 of the Supporting Information). We found that using the blunt edge of a razor blade covered with Kapton tape resulted in the best film quality. Furthermore, heating the blade to ∼155 °C during coating resulted in further improvement of the film quality by preventing solidification of the melt during the deposition. These preliminary blade optimizations led to dramatic improvement in macroscopic uniformity of the film coverage and thickness and eliminated some of the microscopic inhomogeneities observed on the surface of the film. We also found that faster stage translation speeds (the speed at which the substrate moves) of ∼1 mm/s compared to ∼0.5 mm/s resulted in more homogeneous morphology with fewer void spaces observed in SEM images. The morphology of the blade-coated films (Figure 1b) was similar to that of press-coated films (Figure 1a) that were prepared according to the method described by Li et al.[19] Blade- and press-coated films had similar morphologies as viewed from the top down in SEM, both containing microscopic cracks (panels a and b of Figure 1). In contrast, β-Me-PEA_2PbI_4 films prepared by spin coating were smooth in morphology with narrow cracks with limited length that did not penetrate deeply into the film (Figure 1c).

Structure analysis of β-Me-PEA_2PbI_4 films was performed with XRD. As shown in Figure 1d, blade-coated β-Me-PEA_2PbI_4 films consist of a series of {00l} sharp diffraction peaks, indicating that the layers within the RP phase are preferentially oriented in parallel with respect to the substrate. This parallel preferential orientation was common among RP phase perovskite (n = 1) films that are deposited via press coating and spin coating (Figure 1d).[19] Some unidentified small diffraction peaks observed in blade-coated films in our study have also been observed in the past for similar press-coated 2D perovskites.[19] The absorptance spectra of spin-coated β-Me-PEA_2PbI_4 thin films have a sharp excitonic peak at 2.45 eV (Figure 1e). An excitonic peak at 2.45 eV was observed for blade- and press-coated films; however, the peak was broadened and slightly shifted by ∼0.01 eV. The direction of the shift varied randomly between samples (Figure S5b of the Supporting Information) among multiple blade-coated films under nominally identical deposition parameters. The apparent broadening of the excitonic feature in the press-coated film may be due to the large thickness of this sample or a higher defect density. This could be determined using an improved melt-deposition process that enables thinner films. The macroscopic morphologies of these films were similar (Figure S5a of the Supporting Information), and XRD peaks were in the same positions but with different intensities (Figure S5c of the Supporting Information). The inconsistency in broadening and peak shifts could arise from structural,[39] compositional,[40−42] and energetic[43] disorders. It is possible that the change in the absorptance spectra arises from evaporation of the RNH_3^+ cation and/or halide from the film during heating, which could result in the formation of ion impurities. Thus, the observed variation in optical properties could arise from factors that influence degradation or sublimation kinetics of the precursor that are not well-controlled. We note that failure to recover sublimated β-Me-PEA may represent an environmental risk factor; however, it may be more economical to recover β-Me-PEA as a result of its low vapor pressure near room temperature. The factors that control these kinetics are unclear but could be related to deposition conditions, such as the mesh size or packing density of the powder prior to melting or total surface area covered by the powder. It could also be due to non-idealities associated with our blade deposition apparatus, which did not have a precisely controlled translation speed nor a finely adjustable blade angle nor height.

To transform β-Me-PEA_2PbI_4 films into lower bandgap halide perovskite films, we adapted an established A-site cation-exchange approach[25,32,33] to exchange the β-Me-PEA^+ cation with either MA^+ or FA^+. Briefly, β-Me-PEA_2PbI_4 films were placed into a MAI or FAI solution in IPA (10 mg/mL), as illustrated in Scheme 1b. The films were placed in the solution for times ranging from 1 min to 8 h, then rinsed in neat IPA, dried under N_2 flow, and placed on a hot plate at 70 °C for 5 min to form halide perovskites (Scheme 1c). As shown in Figure 2, the color of the spin-coated films transformed from yellow to brown within 1 min of immersing into either MAI or FAI solutions, consistent with the formation of halide perovskite phases and/or RP phases with higher n values. The absorptance spectra indicate a shift in the band gap to lower energies during cation exchange, consistent with transformation to their corresponding halide perovskite phases

https://doi.org/10.1021/acs.jpclett.2c03916
J. Phys. Chem. Lett. 2023, 14, 5194−5202

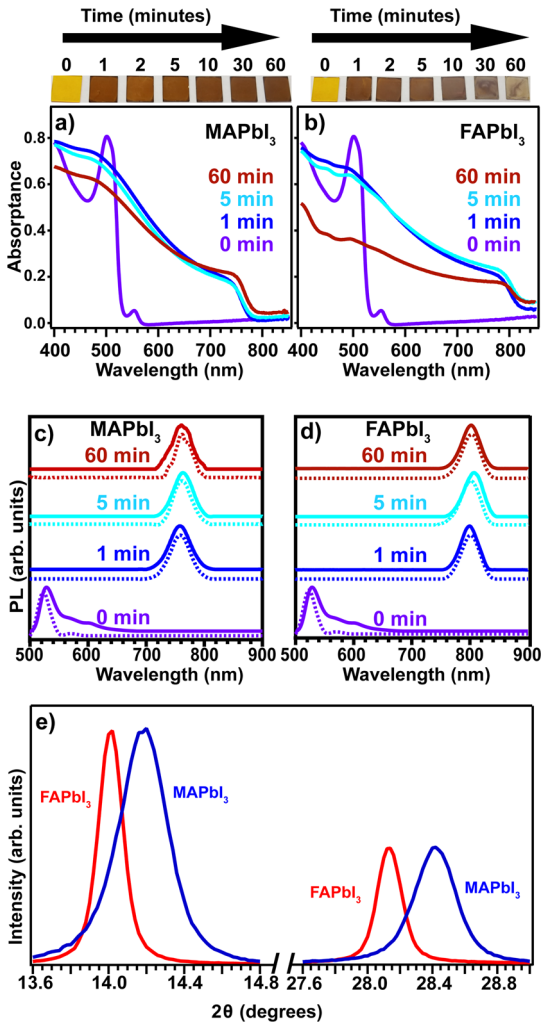

Figure 2. Absorptance and PL spectra (normalized) of spin-coated β-Me-PEA_2PbI_4 thin films followed by cation exchange in 10 mg/mL (a and c) MAI and (b and d) FAI solutions and (e) XRD patterns of spin-coated β-Me-PEA_2PbI_4 thin films after immersion in MAI and FAI solutions for 5 min. The XRD is focused around peaks located at ~14° and ~28° 2θ for clarity. Solid lines and dashed lines in panels c and d represent PL measured at the top surface and bottom (through the glass slide), respectively.

($MAPbI_3$ or $FAPbI_3$).[25,32,33] For films placed in MAI solutions for 5 and 60 min, the band edge reached 1.59 eV (780 nm) and 1.55 eV (795 nm), respectively, agreeing well with the bulk $MAPbI_3$ bandgap.[25] We observed a similar transformation when FAI solutions were used. The band edge appeared at ~1.48 eV (840 nm), consistent with the formation of perovskite phase α-$FAPbI_3$ ("black" phase) after 5 min of immersion. However, when the cation-exchange procedure exceeded 10 min, the films lightened in color and absorptance intensity gradually decreased (Figure 2b), suggesting the instability of the perovskite phase and formation of non-perovskite phase δ-$FAPbI_3$ ("yellow" phase).[44,45] XRD of the films after cation exchange (Figure 2e and Figure S6a of the Supporting Information) shows that both samples have sharp diffraction peaks at ~14.2° corresponding to the (110) Bragg diffraction peak of tetragonal $MAPbI_3$[46] and 14° corresponding to the (101) Bragg diffraction peak of trigonal $FAPbI_3$ ("black phase"),[47] respectively. We did not observe any diffraction peaks corresponding to β-Me-PEA_2PbI_4 in either of these samples, suggesting that the precursor completely transformed to the corresponding perovskite phases (Figure S6b of the Supporting Information). XRD also confirms that $FAPbI_3$ thin films were not pure black phase. A diffraction peak at 11.8°, which is known to arise from the non-perovskite δ phase[47] appeared in all of the samples.[47] With the increase of the FAI solution concentration to 20 mg/mL, the relative intensity of the diffraction peak for δ-$FAPbI_3$ decreased (Figure S7 of the Supporting Information), indicating that the formation of this phase could be minimized by optimizing the solution concentration and immersion time.

We performed room-temperature PL spectroscopy on spin-coated thin films on both coated (front) and glass (back) sides to further study the transformation of two-dimensional (2D) materials into the perovskite phase. All converted thin films showed PL, and the peak maximum shifted to lower energy when increasing the immersion time for both MAI and FAI solutions (panels c and d of Figure 2). This shift was consistent with the shift in band gap observed in the absorptance spectra.[25] We did not notice any difference in PL position when the light was exposed on the front (solid line) or back (dashed line) side of converted $MAPbI_3$ thin films, indicating homogeneous transformation into the perovskite phase throughout the film thickness.[48] However, we noticed that the PL intensities associated with $MAPbI_3$ decreased by increasing the immersion time to 60 min, observed from front and back sides (Figure S8 of the Supporting Information). This implies that, even though there is no discernible change to the 60 min MAPbI3 sample when characterizing its absorptance spectrum or XRD pattern, these PL data indicate increased non-radiative charge carrier recombination deep within the films upon prolonged exposure to the MAI solutions. In the case of thin films that were converted to $FAPbI_3$, we noticed the slight shift in the PL peak for front and back sides for the immersion time of 5 min, implying a formation of RP phases with higher n values at the surface near the glass side. Similar to transformed $MAPbI_3$, a red shift in bandgap was also observed for transformed $FAPbI_3$ films (Figure 2c). However, the kinetics of this process appears to occur much faster to exchange to $FAPbI_3$, which is surprising because FA^+ is much larger than MA^+ (2.53 versus 2.17 Å)[49] and would be expected to have lower diffusivity. While the rationale for why these exchange processes occur at such different rates is an area of ongoing investigation, these results suggest that the exposure time to cation solutions should be optimized for each system to impart optimal optoelectronic behavior.

We also attempted A-site cation exchange on blade-coated samples by placing these films in MAI or FAI solutions in IPA (10 mg/mL) for different periods of time. After 5 min of immersion in MAI solution, the XRD pattern (Figure 3a) shows diffraction peaks that correspond to both β-Me-PEA_2PbI_4 and $MAPbI_3$, indicating incomplete transformation. We also noted that the diffraction peaks are broadened for $MAPbI_3$, which may suggest small grain size, lattice strain, or lower crystallinity.[25,50] Similar incomplete transformation was also observed when blade-coated films were immersed in 10 mg/mL FAI solution for 5 min. Although absorptance spectra show the transformation of β-Me-PEA_2PbI_4 to α-$FAPbI_3$ by shifting the bandgap to lower energy (Figure 3d), the XRD pattern (Figure 3a) indicates the formation of α-$FAPbI_3$ and δ-$FAPbI_3$ phases along with residues of β-Me-PEA_2PbI_4. This incomplete transformation was apparent upon visual inspec-

https://doi.org/10.1021/acs.jpclett.2c03916
J. Phys. Chem. Lett. 2023, 14, 5194−5202

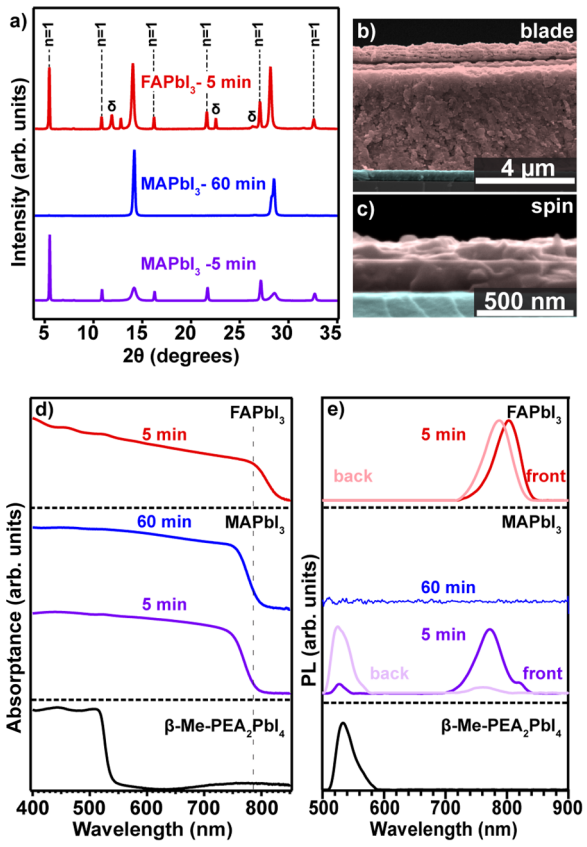

Figure 3. (a) XRD of blade-coated films immersed in MAI and FAI solutions, (b and c) cross-sectional SEM images of blade- and spin-coated films followed by cation exchange in MAI solutions for 5 min, and (d) absorptance and (e) PL spectra (normalized for clarity) of blade-coated films followed by cation exchange in MAI and FAI solutions. δ in panel a denotes non-perovskite δ-$FAPbI_3$. Red shading in panels b and c indicates the perovskite layer, and blue shading indicates the ITO substrate. A dotted line was added to panel d to guide the eye.

tion of the substrates; while the top of the coated side of blade-coated samples appeared brown after immersing in MAI solution, the inner layer of the sample did not appear to transform, retaining the orange color of β-Me-PEA_2PbI_4 when viewing through the back of the glass substrate (Figure S9 of the Supporting Information). This incomplete transformation is likely due to the blade-coated films being substantially thicker. Figure 3b shows a SEM cross section of a blade-coated sample with a thickness of ~5 μm; however, the films are macroscopically inhomogeneous, as shown in photographs (Figure S3 of the Supporting Information), and the thickness of the best films varies between 2 and 10 μm. In contrast, the spin-coated films were uniformly thick, with an average thickness of ~0.25 μm (Figure 3c). As a result of the difference in the thickness, we believe that, within the 5 min immersion time, the cation exchange between MA^+ and β-Me-PEA^+ only occurred at the interface between MAI and blade-coated β-Me-PEA_2PbI_4 films;[51] hence, a longer exposure time is required to transform to the bulk materials.[25,51,52] With the increase of the immersion time in MAI solution to 60 min (Figure 3a), the {00l} diffraction peaks corresponding to β-Me-PEA_2PbI_4 almost disappeared and the intense and narrower diffraction peaks for $MAPbI_3$ were observed, suggesting a larger grain size, reduced strain, or better crystallinity in the samples.[25,50] Absorptance spectra also confirmed the transformation of blade-coated β-Me-PEA_2PbI_4 to $MAPbI_3$. As shown in Figure 3d, the bandgap red shifted to 1.53 eV, similar to the results observed for transformed spin-coated samples (Figure 2a). It should be noted that a longer immersion time (>5 min) in FAI solutions for blade-coated films was avoided because a longer immersion time resulted in apparent loss of color in spin-coated samples (Figure 2b), as they became hazier yellow at increased immersion times.

PL spectra indicated a red shift for blade-coated β-Me-PEA_2PbI_4 films when they were immersed in MAI and FAI solutions for 5 min (Figure 3e). Unlike to spin-coated thin films, we found a difference in the PL peak position when taken from the coated and glass sides, implying inhomogeneous transformation of β-Me-PEA_2PbI_4 to the perovskite phases. PL is in good agreement with the XRD results that β-Me-PEA_2PbI_4 is still present within the film after 5 min of immersing in the MAI solution. However, while XRD results showed that longer immersion times in MAI (60 min) improve conversion, PL was no longer detectable. This implies that prolonged exposure to the MAI solution results in the formation of defects that promote non-radiative carrier recombination.

We performed SEM to study the effect of cation exchange on a film morphology. Spin-coated β-Me-PEA_2PbI_4 films were continuous and pinhole-free with a lateral grain size of ~1.5 μm (Figure 4a). Upon immersion in MAI solution, the grain shape changed, the average grain size became smaller (~0.13 μm), and small cracks were observed (Figure 4b). However, the thin films were still uniform in thickness and microscopically continuous (Figure 4b). Our attempt to perform cation exchange to transform to $FAPbI_3$ resulted in discontinuous morphology with larger grains (roughly average size of ~0.2 μm) compared to the $MAPbI_3$ thin film. We also noticed a needle-like structure on top of the perovskite layer in $FAPbI_3$ thin films (Figure 4c). This observation agrees well with previous findings from Binek et al.,[53] who observed that δ-$FAPbI_3$ tends to adopt a needle-like morphology at room temperature. Given that δ-$FAPbI_3$ impurity was observed in XRD (Figure 3a), we believe that these needle-like features are δ-$FAPbI_3$. Similar patterns in grain size reduction were observed when blade-coated films were immersed in MAI (60 min) and FAI (5 min) solutions (panels d–f of Figure 4). The blade-coated films immersed in MAI solutions had smaller grains compared to the spin-coated samples (panels b and e of Figure 4). A higher concentration of needle-like structures was observed upon transformation of blade-coated β-Me-PEA_2PbI_4 films to $FAPbI_3$ compared to spin-coated thin films (panels c and f of Figure 4). This may be due to a higher concentration of δ-$FAPbI_3$, which is supported with XRD results that show a greater intensity of δ-$FAPbI_3$ reflections (Figure 3a). Despite the feasibility of this melt-processing and cation-exchange approach on blade-coated samples, obtaining uniform surface coverage is still challenging (Figure S10 of the Supporting Information) and would require optimization to construct working devices.

As another alternative to an alcohol-based A-site cation exchange, we also attempted to transform the β-Me-PEA_2PbI_4 films into a halide perovskite phase using a solid-state method. Solid-state synthetic methods for synthesizing halide perovskites and related materials have been well-studied,[47,54–56] typically using routes of heating or mechanochemical grinding of solid powders to form perovskite phases. These approaches

https://doi.org/10.1021/acs.jpclett.2c03916
J. Phys. Chem. Lett. 2023, 14, 5194–5202

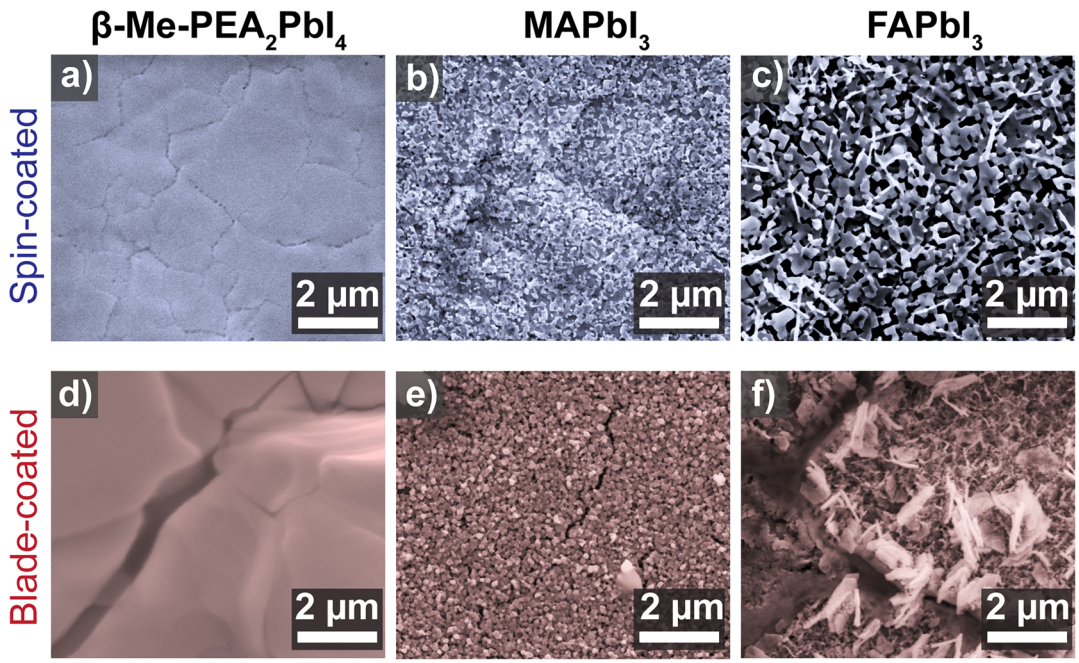

Figure 4. Plan-view SEM images (false color) of (a–c) spin-coated and (d–f) blade-coated β-Me-PEA_2PbI_4 films (a and d) before and after cation exchange in 10 mg/mL (b and e) MAI and (c and f) FAI solutions. All samples were placed in cation solutions for 5 min, except blade-coated samples in MAI solution for 60 min (e).

would usually require air-toxic solvents to transform perovskite powders into thin films. Hence, we modified the thermal annealing method developed by Rosales et al.[57] that heated mixed precursors in air to 50–200 °C to form organolead mixed halides. Here, we put β-Me-PEA_2PbI_4 films in contact with solid MAI by placing MAI powder on top of the β-Me-PEA_2PbI_4 films followed by subsequent heating to 100 °C for 72 h (Figure 5a). As shown in Figure 5b, $MAPbI_3$ was formed during the solid-state reaction, supported by the shoulder in the absorptance spectrum at ~1.5 eV. Other small peaks and shoulders in the absorptance spectrum indicate the formation of other layers (β-Me-$PEA'_2MA_{n-1}Pb_nI_{3n+1}$, with n = 1, 2, 3, etc.).[12,58,59] We noticed that all of the optical features for all layers were shifted to higher energy compared to their pure phases,[12,60] which could be explained by peak convolutions in the mixed phases. XRD (Figure 5c) indicates the formation of tetragonal $MAPbI_3$[61] in the solid-state thin films. However, there are traces of MAI,[44] PbI_2, and β-Me-$PEA_2MA_{n-1}Pb_nI_{3n+1}$ implying that the β-Me-PEA^+ cation is largely retained within the film (Figure S11 of the Supporting Information). Because the solid-state reaction occurs at the interface, we suspect that the interfacial contact area in our process is limited. To test our hypothesis and enhance the interfacial area, we ground MAI and β-Me-PEA_2PbI_4 powders and heated them at 100 °C for 48 h in a box furnace in air. We noted similar transformation to $MAPbI_3$ with residual PbI_2; however, the diffraction peaks for β-Me-PEA_2PbI_4 disappeared and decreased for other phases compared to the sample where MAI was only placed on the top surface (Figure S12 of the Supporting Information). We believe that there are many factors that could play a role in limiting the reaction. For example, the success of solid-state reactions heavily depends upon the diffusion rate of reactive species;[56] therefore, increasing the reaction temperature could increase the diffusion rate[62] for A-site cation exchange.[51] It is also known that the diffusion length would impact the reaction rate, and for that reason, the mixed powders were usually

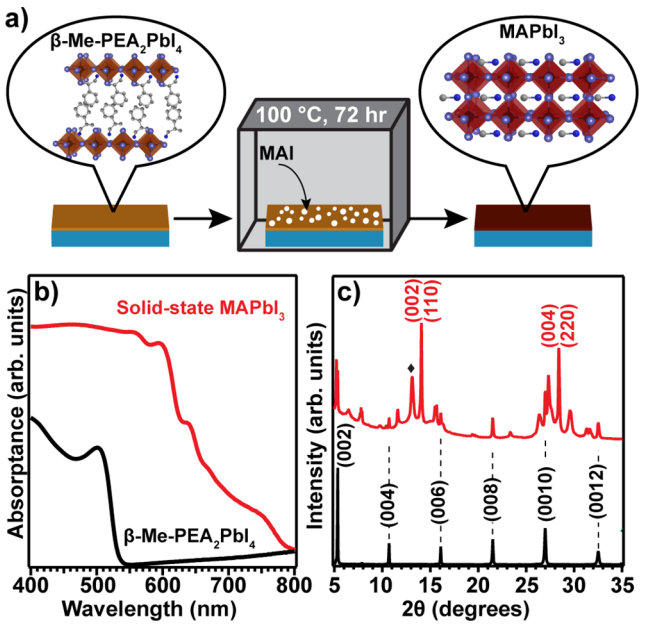

Figure 5. (a) Schematic of the solid-state reaction between β-Me-PEA_2PbI_4 and MAI and (b) absorptance spectra and (c) XRD results of the blade-coated β-Me-PEA_2PbI_4 film before (black) and after (red) the solid-state reaction. Reference patterns in panel c were simulated from reference patterns for $MAPbI_3$[61] and PbI_2.[64] The peak marked with ♦ denotes a reflection associated with PbI_2.

pelletized to reduce the diffusion path.[62] Using thinner β-Me-PEA_2PbI_4 films may also be useful to reduce the diffusion path and enhance the transformation rate. Finally, using a different reaction vessel may also improve transformation. Many solid-state methods for synthesizing halide perovskites were conducted in a sealed tube to avoid loss of organic components.[63]

https://doi.org/10.1021/acs.jpclett.2c03916
J. Phys. Chem. Lett. 2023, 14, 5194–5202

The use of air-toxic solvents for depositing halide perovskite thin films poses an industrial challenge toward the commercial viability of perovskite solar cells and other wide-area devices. We conclude that melt-based processing is a promising alternative route for fabricating layered lead halide perovskite films that can lead to liquid-processed halide perovskite thin films without using air-toxic solvents. We demonstrated that films of β-Me-PEA_2PbI_4 could be deposited using melt-processed blade coating, subsequently transformed into a halide perovskite phase using A-site cation exchange. We gained insight into the kinetics of this cation-exchange process in both spin- and blade-coated films. In the thinner, more compact spin-coated β-Me-PEA_2PbI_4 films, complete and homogeneous cation exchange occurred within minutes. In contrast, the thicker blade-coated samples resulted in slower transformation to $MAPbI_3$. We also showed that both spin- and blade-coated films transformed to α-$FAPbI_3$ upon exposure to FAI solutions, with an increasing amount of a δ-$FAPbI_3$ impurity with greater exposure times. Melt-processable β-Me-PEA_2PbI_4 was partially transformed into $MAPbI_3$ films using a solid-state reaction, with a resulting film that had broad visible light absorption. Future work to improve the blade-coating morphology and substrate coverage, combined with a further optimized solvent-free solid-state cation exchange, could result in a route to highly efficient halide perovskite devices. Furthermore, several advances in the chemistry of layered hybrid lead halide perovskites have resulted in new phases with lower melting temperature, such as organic ammonium cation branching.[3] The simplicity of these approaches combined with this environmentally friendly liquid-phase deposition mitigates the use of air-toxic solvents from the thin-film fabrication process and suggests their potential use in large-scale, economical optoelectronic devices.

■ ASSOCIATED CONTENT

Supporting Information

The Supporting Information is available free of charge at https://pubs.acs.org/doi/10.1021/acs.jpclett.2c03916.

Materials and Methods, experimental setup apparatus, photographs, SEM images, optical absorptance, and XRD of blade-coated thin films before and after cation exchange, XRD pattern for solid-state $MAPbI_3$ (powder), and reference XRD pattern for $MAPbI_3$, $FAPbI_3$, and PbI_2 (PDF)

■ AUTHOR INFORMATION

Corresponding Author

Matthew G. Panthani − *Department of Chemical and Biological Engineering, Iowa State University, Ames, Iowa 50011, United States;* orcid.org/0000-0002-3795-2051; Email: panthani@iastate.edu

Authors

Atefe Hadi − *Department of Chemical and Biological Engineering, Iowa State University, Ames, Iowa 50011, United States;* orcid.org/0000-0002-1682-1757

Rainie L. Schlichtmann − *Department of Chemical and Biological Engineering, Iowa State University, Ames, Iowa 50011, United States;* orcid.org/0000-0003-1335-0002

Matthew I. Milot − *Department of Chemical and Biological Engineering, Iowa State University, Ames, Iowa 50011, United States*

Jonathan Slobidsky − *Department of Chemical and Biological Engineering, Iowa State University, Ames, Iowa 50011, United States*

Madeleine Wilsey − *Ames Laboratory, United States Department of Energy, Ames, Iowa 50011, United States;* orcid.org/0000-0003-4680-8163

Alex Verburg − *Department of Chemical and Biological Engineering, Iowa State University, Ames, Iowa 50011, United States*

Yunhua Chen − *Department of Chemistry, Iowa State University, Ames, Iowa 50011, United States*

Umar H. Hamdeh − *Department of Chemical and Biological Engineering, Iowa State University, Ames, Iowa 50011, United States;* orcid.org/0000-0001-7912-2032

Bradley J. Ryan − *Department of Chemical and Biological Engineering, Iowa State University, Ames, Iowa 50011, United States;* orcid.org/0000-0002-7719-5593

Brett Boote − *Chemical Instrumentation Facility, Iowa State University, Ames, Iowa 50011, United States*

Javier Vela − *Ames Laboratory, United States Department of Energy, Ames, Iowa 50011, United States; Department of Chemistry, Iowa State University, Ames, Iowa 50011, United States;* orcid.org/0000-0001-5124-6893

Complete contact information is available at: https://pubs.acs.org/10.1021/acs.jpclett.2c03916

Notes

The authors declare no competing financial interest.

■ ACKNOWLEDGMENTS

The authors thank Carolina Selvati for assisting us in collecting XRD patterns and Warren Straszheim for useful discussions while collecting SEM images. This work was partially supported by funding from the Air Force Office of Scientific Research Grant FA9550-20-1-0018 and the National Science Foundation CAREER Award (DMR-1847370). Atefe Hadi acknowledges funding support from the Catron Foundation. Rainie L. Schlichtmann and Bradley J. Ryan acknowledge funding support from the National Science Foundation Graduate Research Fellowship Program under Grant DGE 1744592. Madeleine Wilsey is grateful to the Ames Laboratory and the U.S. Department of Energy Office of Science for the Science Undergraduate Laboratory Internship under its contract with Iowa State University (Contract DE-AC02-07CH11358). Matthew I. Milot acknowledges funding from the National Science Foundation for Louis Stokes Alliances for Minority Participation Program (HRD-1619654). Jonathan Slobidsky acknowledges funding support from the Griswold Undergraduate Research Internship Program. Javier Vela thanks the U.S. National Science Foundation for a grant from the Division of Chemistry, Macromolecular, Supramolecular, and Nanochemistry Program (1905066). Matthew G. Panthani acknowledges support from the Herbert L. Stiles Faculty Fellowship.

■ REFERENCES

(1) Eperon, G. E.; Hörantner, M. T.; Snaith, H. J. Metal halide perovskite tandem and multiple-junction photovoltaics. *Nat. Rev. Chem.* **2017**, *1* (12), 0095.

(2) Chen, B.; Zheng, X.; Bai, Y.; Padture, N. P.; Huang, J. Progress in tandem solar cells based on hybrid organic−inorganic perovskites. *Adv. Energy Mater.* **2017**, *7* (14), 1602400.

(3) García de Arquer, F. P.; Armin, A.; Meredith, P.; Sargent, E. H. Solution-processed semiconductors for next-generation photodetectors. *Nat. Rev. Mater.* **2017**, *2* (3), 16100.
(4) Quan, L. N.; Rand, B. P.; Friend, R. H.; Mhaisalkar, S. G.; Lee, T.-W.; Sargent, E. H. Perovskites for next-generation optical sources. *Chem. Rev.* **2019**, *119* (12), 7444−7477.
(5) Veldhuis, S. A.; Boix, P. P.; Yantara, N.; Li, M.; Sum, T. C.; Mathews, N.; Mhaisalkar, S. G. Perovskite materials for light-emitting diodes and lasers. *Adv. Mater.* **2016**, *28* (32), 6804−6834.
(6) Zhang, W.; Eperon, G. E.; Snaith, H. J. Metal halide perovskites for energy applications. *Nat. Energy* **2016**, *1* (6), 16048.
(7) Li, B.; Hui, W.; Ran, X.; Xia, Y.; Xia, F.; Chao, L.; Chen, Y.; Huang, W. Metal halide perovskites for resistive switching memory devices and artificial synapses. *J. Mater. Chem. C* **2019**, *7* (25), 7476−7493.
(8) Green, M. A.; Ho-Baillie, A. Perovskite solar cells: The birth of a new era in photovoltaics. *ACS Energy Lett.* **2017**, *2* (4), 822−830.
(9) Kumawat, N. K.; Swarnkar, A.; Nag, A.; Kabra, D. Ligand engineering to improve the luminance efficiency of CsPbBr3 nanocrystal based light-emitting diodes. *J. Phys. Chem. C* **2018**, *122* (25), 13767−13773.
(10) United States Environmental Protection Agency (U.S. EPA). *Initial List of Hazardous Air Pollutants with Modifications*; U.S. EPA: Washington, D.C., 2023; https://www.epa.gov/haps/initial-list-hazardous-air-pollutants-modifications (accessed Feb 14, 2023).
(11) Mitzi, D. B. A layered solution crystal growth technique and the crystal structure of $(C_6H_5C_2H_4NH_3)_2PbCl_4$. *J. Solid State Chem.* **1999**, *145* (2), 694−704.
(12) Smith, I. C.; Hoke, E. T.; Solis-Ibarra, D.; McGehee, M. D.; Karunadasa, H. I. A layered hybrid perovskite solar-cell absorber with enhanced moisture stability. *Angew. Chem.* **2014**, *126* (42), 11414−11417.
(13) Cao, D. H.; Stoumpos, C. C.; Farha, O. K.; Hupp, J. T.; Kanatzidis, M. G. 2D homologous perovskites as light-absorbing materials for solar cell applications. *J. Am. Chem. Soc.* **2015**, *137* (24), 7843−7850.
(14) Mitzi, D. B.; Feild, C. A.; Harrison, W. T. A.; Guloy, A. M. Conducting tin halides with a layered organic-based perovskite structure. *Nature* **1994**, *369* (6480), 467−469.
(15) Mitzi, D. B.; Chondroudis, K.; Kagan, C. R. Design, Structure, and Optical Properties of Organic−Inorganic Perovskites Containing an Oligothiophene Chromophore. *Inorg. Chem.* **1999**, *38* (26), 6246−6256.
(16) Mitzi, D. B.; Medeiros, D. R.; DeHaven, P. W. Low-Temperature Melt Processing of Organic− Inorganic Hybrid Films. *Chem. Mater.* **2002**, *14* (7), 2839−2841.
(17) Li, T.; Dunlap-Shohl, W. A.; Reinheimer, E. W.; Le Magueres, P.; Mitzi, D. B. Melting temperature suppression of layered hybrid lead halide perovskites via organic ammonium cation branching. *Chem. Sci.* **2019**, *10* (4), 1168−1175.
(18) Li, T.; Zeidell, A.; Findik, G.; Dunlap-Shohl, W. A.; Euvrard, J.; Gundogdu, K.; Jurchescu, O. D.; Mitzi, D. B. Phase-pure Hybrid Layered Lead Iodide Perovskite Films Based on A Two-Step Melt Processing Approach. *Chem. Mater.* **2019**, *31* (11), 4267−4274.
(19) Li, T.; Dunlap-Shohl, W. A.; Han, Q.; Mitzi, D. B. Melt processing of hybrid organic−inorganic lead iodide layered perovskites. *Chem. Mater.* **2017**, *29* (15), 6200−6204.
(20) Mitzi, D. B. Solution-processed inorganic semiconductors. *J. Mater. Chem.* **2004**, *14* (15), 2355−2365.
(21) Mitzi, D. B.; Medeiros, D. R.; Malenfant, P. R. L. Intercalated organic− inorganic perovskites stabilized by fluoroaryl− aryl interactions. *Inorg. Chem.* **2002**, *41* (8), 2134−2145.
(22) Zhang, X.; Munir, R.; Xu, Z.; Liu, Y.; Tsai, H.; Nie, W.; Li, J.; Niu, T.; Smilgies, D.-M.; Kanatzidis, M. G.; Mohite, A. D.; Zhao, K.; Amassian, A.; Liu, S. F. Phase transition control for high performance Ruddlesden−Popper perovskite solar cells. *Adv. Mater.* **2018**, *30* (21), 1707166.
(23) Tsai, H.; Nie, W.; Blancon, J.-C.; Stoumpos, C. C.; Asadpour, R.; Harutyunyan, B.; Neukirch, A. J.; Verduzco, R.; Crochet, J. J.; Tretiak, S.; Pedesseau, L.; Even, J.; Alam, M. A.; Gupta, G.; Lou, J.; Ajayan, P. M.; Bedzyk, M. J.; Kanatzidis, M. G.; Mohite, A. D. High-efficiency two-dimensional Ruddlesden−Popper perovskite solar cells. *Nature* **2016**, *536* (7616), 312−316.
(24) Hills-Kimball, K.; Nagaoka, Y.; Cao, C.; Chaykovsky, E.; Chen, O. Synthesis of formamidinium lead halide perovskite nanocrystals through solid−liquid−solid cation exchange. *J. Mater. Chem. C* **2017**, *5* (23), 5680−5684.
(25) Eperon, G. E.; Beck, C. E.; Snaith, H. J. Cation exchange for thin film lead iodide perovskite interconversion. *Mater. Horiz.* **2016**, *3* (1), 63−71.
(26) Yu, D.; Cai, B.; Cao, F.; Li, X.; Liu, X.; Zhu, Y.; Ji, J.; Gu, Y.; Zeng, H. Cation Exchange-Induced Dimensionality Construction: From Monolayered to Multilayered 2D Single Crystal Halide Perovskites. *Adv. Mater. Interfaces* **2017**, *4* (19), 1700441.
(27) Ji, F.; Wang, L.; Pang, S.; Gao, P.; Xu, H.; Xie, G.; Zhang, J.; Cui, G. A balanced cation exchange reaction toward highly uniform and pure phase FA 1− x MA x PbI 3 perovskite films. *J. Mater. Chem. A* **2016**, *4* (37), 14437−14443.
(28) Jiang, Y.; Leyden, M. R.; Qiu, L.; Wang, S.; Ono, L. K.; Wu, Z.; Juarez-Perez, E. J.; Qi, Y. Combination of Hybrid CVD and Cation Exchange for Upscaling Cs-Substituted Mixed Cation Perovskite Solar Cells with High Efficiency and Stability. *Adv. Funct. Mater.* **2018**, *28* (1), 1703835.
(29) Zhao, T.; Liu, H.; Ziffer, M. E.; Rajagopal, A.; Zuo, L.; Ginger, D. S.; Li, X.; Jen, A. K. Y. Realization of a highly oriented MAPbBr3 perovskite thin film via ion exchange for ultrahigh color purity green light emission. *ACS Energy Lett.* **2018**, *3* (7), 1662−1669.
(30) Zhou, Y.; Yang, M.; Pang, S.; Zhu, K.; Padture, N. P. Exceptional morphology-preserving evolution of formamidinium lead triiodide perovskite thin films via organic-cation displacement. *J. Am. Chem. Soc.* **2016**, *138* (17), 5535−5538.
(31) Niemann, R. G.; Gouda, L.; Hu, J.; Tirosh, S.; Gottesman, R.; Cameron, P. J.; Zaban, A. Cs^+ incorporation into $CH_3NH_3PbI_3$ perovskite: Substitution limit and stability enhancement. *J. Mater. Chem. A* **2016**, *4* (45), 17819−17827.
(32) Koh, T. M.; Shanmugam, V.; Schlipf, J.; Oesinghaus, L.; Müller-Buschbaum, P.; Ramakrishnan, N.; Swamy, V.; Mathews, N.; Boix, P. P.; Mhaisalkar, S. G. Nanostructuring Mixed-Dimensional Perovskites: A Route Toward Tunable, Efficient Photovoltaics. *Adv. Mater.* **2016**, *28* (19), 3653−3661.
(33) Adjokatse, S.; Fang, H.-H.; Duim, H.; Loi, M. A. Scalable fabrication of high-quality crystalline and stable FAPbI 3 thin films by combining doctor-blade coating and the cation exchange reaction. *Nanoscale* **2019**, *11* (13), 5989−5997.
(34) Wu, P.; He, Q.; Zhu, D.; Jiang, H.; Jiao, Z.; Zhang, Y.; Xu, W.; Fu, Y.; Cao, H.; Cheng, J. Highly efficient fluorescent and colorimetric sensing of organic amine vapors based on organometal halide perovskite nanostructures. *Anal. Methods* **2017**, *9* (25), 3804−3809.
(35) Xie, A.; Maddalena, F.; Witkowski, M. E.; Makowski, M.; Mahler, B.; Drozdowski, W.; Springham, S. V.; Coquet, P.; Dujardin, C.; Birowosuto, M. D.; Dang, C. Library of Two-Dimensional Hybrid Lead Halide Perovskite Scintillator Crystals. *Chem. Mater.* **2020**, *32* (19), 8530−8539.
(36) Li, Y.; Shao, W.; Ouyang, X.; Zhu, Z.; Zhang, H.; Ouyang, X.; Liu, B.; Xu, Q. Scintillation properties of perovskite single crystals. *J. Phys. Chem. C* **2019**, *123* (28), 17449−17453.
(37) Chen, H.; Zhang, M.; Bo, R.; Barugkin, C.; Zheng, J.; Ma, Q.; Huang, S.; Ho-Baillie, A. W. Y.; Catchpole, K. R.; Tricoli, A. Superior self-powered room-temperature chemical sensing with light-activated inorganic halides perovskites. *Small* **2018**, *14* (7), 1702571.
(38) Choi, J.; Park, S.; Lee, J.; Hong, K.; Kim, D.-H.; Moon, C. W.; Park, G. D.; Suh, J.; Hwang, J.; Kim, S. Y.; Jung, H. S.; Park, N.-G.; Han, S.; Nam, K. T.; Jang, H. W. Organolead halide perovskites for low operating voltage multilevel resistive switching. *Adv. Mater.* **2016**, *28* (31), 6562−6567.
(39) Franssen, W. M. J.; van Es, S. G. D.; Dervişoğlu, R.; de Wijs, G. A.; Kentgens, A. P. M. Symmetry, dynamics, and defects in

https://doi.org/10.1021/acs.jpclett.2c03916
J. Phys. Chem. Lett. 2023, 14, 5194−5202

methylammonium lead halide perovskites. *J. Phys. Chem. Lett.* **2017**, *8* (1), 61−66.
(40) Baranovskii, S. D.; Doerr, U.; Thomas, P.; Naumov, A.; Gebhardt, W. Exciton line broadening by compositional disorder in alloy quantum wells. *Phys. Rev. B* **1993**, *48* (23), 17149.
(41) Bi, Z.; Rodríguez-Martínez, X.; Aranda, C.; Pascual-San-José, E.; Goñi, A. R.; Campoy-Quiles, M.; Xu, X.; Guerrero, A. Defect tolerant perovskite solar cells from blade coated non-toxic solvents. *J. Mater. Chem. A* **2018**, *6* (39), 19085−19093.
(42) Rahimnejad, S.; Kovalenko, A.; Forés, S. M.; Aranda, C.; Guerrero, A. Coordination Chemistry Dictates the Structural Defects in Lead Halide Perovskites. *ChemPhysChem* **2016**, *17* (18), 2795−2798.
(43) Straus, D. B.; Iotov, N.; Gau, M. R.; Zhao, Q.; Carroll, P. J.; Kagan, C. R. Longer cations increase energetic disorder in excitonic 2D hybrid perovskites. *J. Phys. Chem. Lett.* **2019**, *10* (6), 1198−1205.
(44) Prathapani, S.; Choudhary, D.; Mallick, S.; Bhargava, P.; Yella, A. Experimental evaluation of room temperature crystallization and phase evolution of hybrid perovskite materials. *CrystEngComm* **2017**, *19* (27), 3834−3843.
(45) Li, Z.; Yang, M.; Park, J.-S.; Wei, S.-H.; Berry, J. J.; Zhu, K. Stabilizing perovskite structures by tuning tolerance factor: Formation of formamidinium and cesium lead iodide solid-state alloys. *Chem. Mater.* **2016**, *28* (1), 284−292.
(46) Fang, H. H.; Raissa, R.; Abdu-Aguye, M.; Adjokatse, S.; Blake, G. R.; Even, J.; Loi, M. A. Photophysics of organic−inorganic hybrid lead iodide perovskite single crystals. *Adv. Funct. Mater.* **2015**, *25* (16), 2378−2385.
(47) Stoumpos, C. C.; Malliakas, C. D.; Kanatzidis, M. G. Semiconducting tin and lead iodide perovskites with organic cations: Phase transitions, high mobilities, and near-infrared photoluminescent properties. *Inorg. Chem.* **2013**, *52* (15), 9019−9038.
(48) Wygant, B. R.; Ye, A. Z.; Dolocan, A.; Vu, Q.; Abbot, D. M.; Mullins, C. B. Probing the degradation chemistry and enhanced stability of 2D organolead halide perovskites. *J. Am. Chem. Soc.* **2019**, *141* (45), 18170−18181.
(49) Kieslich, G.; Sun, S.; Cheetham, A. K. Solid-state principles applied to organic−inorganic perovskites: New tricks for an old dog. *Chem. Sci.* **2014**, *5* (12), 4712−4715.
(50) Liu, G.; Gong, J.; Kong, L.; Schaller, R. D.; Hu, Q.; Liu, Z.; Yan, S.; Yang, W.; Stoumpos, C. C.; Kanatzidis, M. G.; Mao, H.-k.; Xu, T. Isothermal pressure-derived metastable states in 2D hybrid perovskites showing enduring bandgap narrowing. *Proc. Natl. Acad. Sci. U. S. A.* **2018**, *115* (32), 8076−8081.
(51) Pan, D.; Fu, Y.; Chen, J.; Czech, K. J.; Wright, J. C.; Jin, S. Visualization and studies of ion-diffusion kinetics in cesium lead bromide perovskite nanowires. *Nano Lett.* **2018**, *18* (3), 1807−1813.
(52) Liu, L.; Bai, Y.; Zhang, X.; Shang, Y.; Wang, C.; Wang, H.; Zhu, C.; Hu, C.; Wu, J.; Zhou, H.; Li, Y.; Yang, S.; Ning, Z.; Chen, Q. Cation Diffusion Guides Hybrid Halide Perovskite Crystallization during the Gel Stage. *Angew. Chem., Int. Ed.* **2020**, *59* (15), 5979−5987.
(53) Binek, A.; Hanusch, F. C.; Docampo, P.; Bein, T. Stabilization of the trigonal high-temperature phase of formamidinium lead iodide. *J. Phys. Chem. Lett.* **2015**, *6* (7), 1249−1253.
(54) Prochowicz, D.; Franckevičius, M.; Cieślak, A. M.; Zakeeruddin, S. M.; Grätzel, M.; Lewiński, J. Mechanosynthesis of the hybrid perovskite $CH_3NH_3PbI_3$: Characterization and the corresponding solar cell efficiency. *J. Mater. Chem. A* **2015**, *3* (41), 20772−20777.
(55) Jodlowski, A. D.; Yépez, A.; Luque, R.; Camacho, L.; de Miguel, G. Benign-by-Design Solventless Mechanochemical Synthesis of Three-, Two-, and One-Dimensional Hybrid Perovskites. *Angew. Chem., Int. Ed.* **2016**, *55* (48), 14972−14977.
(56) Rosales, B. A.; Wei, L.; Vela, J. Synthesis and mixing of complex halide perovskites by solvent-free solid-state methods. *J. Solid State Chem.* **2019**, *271*, 206−215.
(57) Rosales, B. A.; Men, L.; Cady, S. D.; Hanrahan, M. P.; Rossini, A. J.; Vela, J. Persistent dopants and phase segregation in organolead mixed-halide perovskites. *Chem. Mater.* **2016**, *28* (19), 6848−6859.
(58) Quan, L. N.; Yuan, M.; Comin, R.; Voznyy, O.; Beauregard, E. M.; Hoogland, S.; Buin, A.; Kirmani, A. R.; Zhao, K.; Amassian, A.; Kim, D. H.; Sargent, E. H. Ligand-stabilized reduced-dimensionality perovskites. *J. Am. Chem. Soc.* **2016**, *138* (8), 2649−2655.
(59) Stamplecoskie, K. G.; Manser, J. S.; Kamat, P. V. Dual nature of the excited state in organic−inorganic lead halide perovskites. *Energy Environ. Sci.* **2015**, *8* (1), 208−215.
(60) Calabrese, J.; Jones, N. L.; Harlow, R. L.; Herron, N.; Thorn, D. L.; Wang, Y. Preparation and characterization of layered lead halide compounds. *J. Am. Chem. Soc.* **1991**, *113* (6), 2328−2330.
(61) Yamada, Y.; Yamada, T.; Phuong, L. Q.; Maruyama, N.; Nishimura, H.; Wakamiya, A.; Murata, Y.; Kanemitsu, Y. Dynamic optical properties of $CH_3NH_3PbI_3$ single crystals as revealed by one- and two-photon excited photoluminescence measurements. *J. Am. Chem. Soc.* **2015**, *137* (33), 10456−10459.
(62) Smart, L. E.; Moore, E. A. *Solid State Chemistry: An Introduction*, 4th ed.; CRC Press: Boca Raton, FL, 2012; DOI: 10.1201/b12047.
(63) Mitzi, D. B.; Liang, K. Preparation and properties of $(C_4H_9NH_3)_2EuI_4$: A luminescent organic− inorganic perovskite with a divalent rare-earth metal halide framework. *Chem. Mater.* **1997**, *9* (12), 2990−2995.
(64) Terpstra, P.; Westenbrink, H. G. K. On the crystal structure of Lead-iodide. *Proc. K. Ned. Akad. Wet.* **1926**, *29*, 431−442.

https://doi.org/10.1021/acs.jpclett.2c03916
J. Phys. Chem. Lett. 2023, 14, 5194−5202